# Faraday Discussions

Accepted Manuscript

## Faraday Discussions

### Royal Society of Chemistry

ROYAL SOCIETY
OF CHEMISTRY

www.rsc.org/faraday_d

# Bioinspired Magnetite Formation from a Disordered Ferrihydrite-Derived Precursor

**Archan Dey[a], Jos J.M. Lenders[a,b] and Nico A.J.M. Sommerdijk[a,b]\***

We show that by reacting ferrihydrite (FeH) with $Fe^{(II)}$ ions and subsequently increasing the pH, magnetite is formed through a multi-step nucleation process mediated by monodisperse $FeH-Fe^{(II)}$ primary particles. The interaction of these primary particles with a transient green rust phase leads to the formation of smaller secondary particles which form the feedstock for magnetite formation. Surprisingly, the presence of a polypeptide additive prevents the formation of green rust as a $Fe^{(II)}$-rich intermediate phase, and leads to the formation of amorphous aggregates of $FeH-Fe^{(II)}$ particles which subsequently transform into the final magnetite nanocrystals. The observation of multiple transitions and the involvement of disordered precursor phases in this bioinspired crystallization route is of importance for our understanding of the nucleation of magnetite in geological and biological environments and may lead to new approaches in the sustainable synthesis of this technologically important mineral.

## 1 Introduction

Magnetite ($Fe_3O_4$) is a widespread ferrimagnetic mineral encountered in many biological and geological systems.[1] It also has a broad array of technological applications, e.g. in magnetic data storage materials, inks, ferrofluids, scavengers in water purification, but also in magnetic resonance imaging and controlled drug delivery.[2-4] The magnetic properties of $Fe_3O_4$ nanoparticles strongly depend on their size and morphology. Consequently, controlling the growth of these crystalline particles is essential to fine-tune their properties for specific applications. As magnetotactic bacteria produce such iron oxide particles under ambient conditions with precisely controlled shape and size,[5] the synthesis of magnetite under biomimetic conditions, i.e. at ambient temperatures and in aqueous media, is now a field of increasing interest.[6] It is clear that only through a detailed understanding of the mechanisms underlying the nucleation and growth in biomimetic magnetite formation the production of optimized magnetite nanoparticles eventually will become feasible.

Magnetotactic bacteria synthesize 30-140 nm magnetite crystals with often elongated morphologies, which are both crystallographically and magnetically aligned in chains.[5] The formation of these nanoparticles takes place in magnetosome vesicles,[5, 7] where their nucleation and growth is controlled through the interaction with a variety of biomolecules. Even though the mechanistic pathway involved has been a topic of debate for many years,[8-10] it was recently established that ferrihydrite is present as a precursor inside the magnetosome vesicle prior to the formation of magnetite.[11-13] Although still many questions remain concerning the exact pathway of magnetite biomineralization, it is clear that it concerns two important steps: 1) the local formation of significant quantities of ferrihydrite and 2) the conversion to magnetite through reaction with $Fe^{(II)}$.

Following our initial report that magnetite can be formed through transient ferrihydrite-like primary particles,[14] we recently developed a bioinspired synthesis route, which allows the formation of ferrimagnetic magnetite nanocrystals from a ferrihydrite precursor.[15] This procedure involves the reaction of ferrihydrite with
5 Fe(II) present in the solution upon increasing the pH through the in-diffusion of ammonia vapor and allows polypeptides to interact with the developing crystals to control their size, shape and dispersibility.[16]

Here we investigate the nucleation of magnetite from a ferrihydrite precursor, separating the addition of Fe(II) from the pH increase by ammonia in-diffusion.
10 Using high-resolution cryo-TEM with selected-area electron diffraction we reveal that the conversion of ferrihydrite to magnetite follows a multi-step process, involving green rust as a transient phase of which the formation and disintegration is mediated by two different populations of 1.5-2.0 nm and 1.0-1.5 nm particles, respectively. Strikingly, the formation of green rust is bypassed through the presence
15 of a random polypeptide of glutamic acid, lysine and alanine monomers, such that magnetite formation now proceeds through an intermediate devoid of any long-range order, consisting of an assembly of these nanoscopic particles.

## 2 Results

Magnetite was synthesized using ferrihyrite (FeH) as a precursor, with the latter
20 obtained from $FeCl_3.6H_2O$ through a modified literature procedure.[17] The obtained gel-like precursor material was identified as 6-line FeH by powder X-ray diffraction (PXRD) after freeze-drying and did not change its crystallinity or phase purity upon storage at 4 °C for a month (**Figure 1a,b**). Cryogenic transmission electron microscopy (cryo-TEM) demonstrated that the gel-like FeH phase consisted of a
25 highly hydrated network of nanometer-sized particles (**Figure 2**).[14] For cryo-TEM, ~100 nm thin films of aqueous samples are rapidly vitrified in liquid ethane (-183 °C) to obtain amorphous ice layers, which subsequently are studied at temperatures low enough to avoid their recrystallization (<-140 °C).[18]
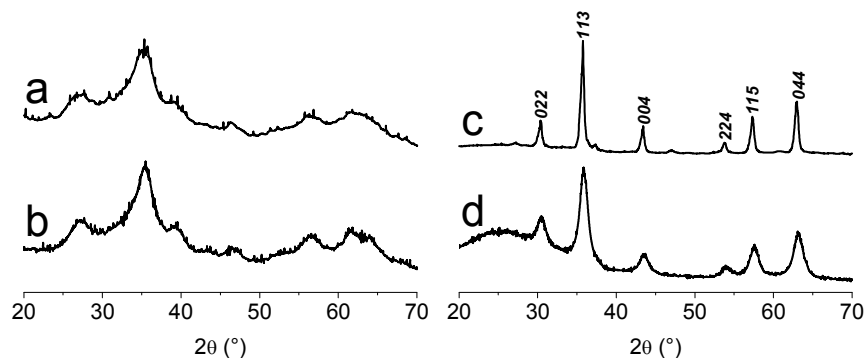


30 **Figure 1:** Powder XRD patterns of freeze-dried samples. (a) Freshly prepared 6-line ferrihydrite (FeH) from $FeCl_3.6H_2O$. (b) FeH stored at 4 °C for a month, showing no signs of altered crystallinity or phase purity. (c) Phase-pure magnetite obtained after 16 hours reaction time without additives. The 6 major reflections are indexed to common $Fe_3O_4$ crystal planes. (d) Phase-pure magnetite obtained after 16 hours reaction time in the presence of the additive **EKA**, showing
35 broader peaks as compared to the control.

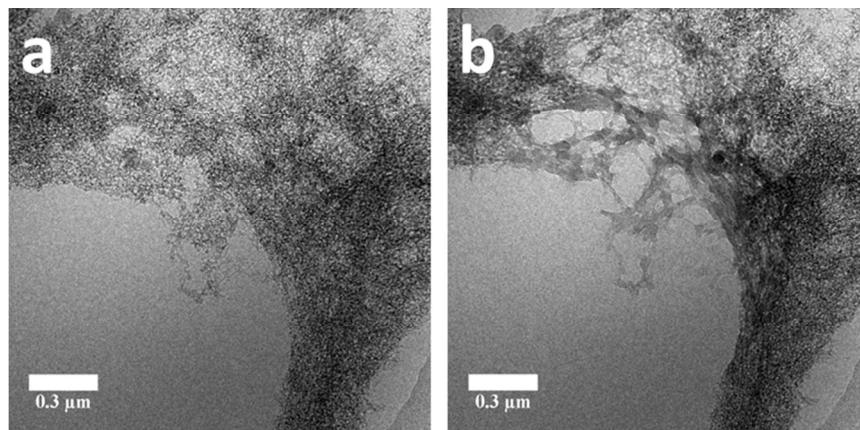**Figure 2:** Cryo-TEM images of the FeH precursor, showing its gel-like character and beam-sensitive nature, (a) and (b) are two subsequent images that were taken from the same area.[14] Reprinted with permission from the Nature Publishing Group, Copyright 2013.

5    The transformation of ferrihydrite to magnetite was carried out by the addition of 0.55 equivalents of $FeCl_2.4H_2O$ under a $N_2$ atmosphere and the subsequent increase of the solution pH by $NH_3$ in-diffusion.[15] Indeed, after 16 hours a black precipitate was isolated for which PXRD showed it was phase-pure magnetite (**Figure 1c**).

   To obtain insight in the mechanism of this conversion process, the development
10 of morphology and structure was monitored using cryo-TEM and low-dose selected-area electron diffraction (SAED), and the pH was monitored with a pH electrode. Upon addition of $Fe^{(II)}$ to the FeH dispersion at pH ~5, cryo-TEM analysis showed the formation of a more monodisperse population of particles with diameters of 1.5-2.0 nm within the initial FeH gel (**Figure 3**), similar to the primary particles
15 observed previously for the controlled coprecipitation of $Fe^{(II)}$ and $Fe^{(III)}$.[14] Also in this case these primary particles did not show any long-range order in SAED (**Figure 3b**, inset), but showed improved stability towards electron beam exposure, meaning that they could resist a higher electron dose before visible damage occurred. This observation suggests that their formation is accompanied by a
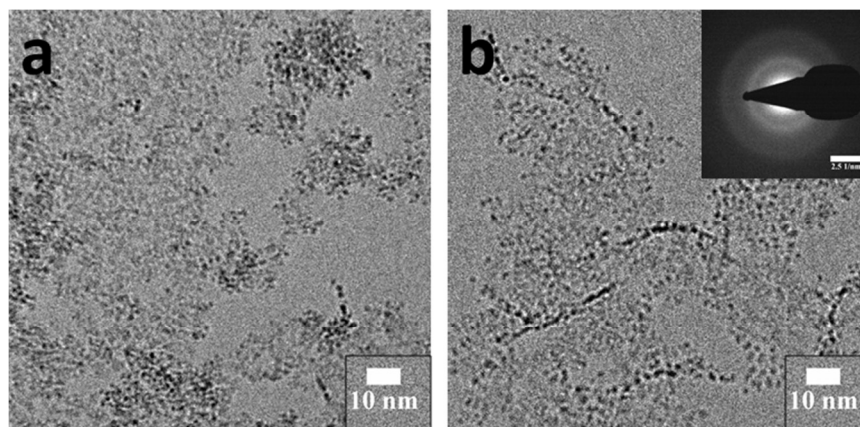20 dehydration of the original FeH gel.

**Figure 3:** Cryo-TEM images of FeH in the presence of Fe$^{(II)}$ at pH ~5, (a) and (b) are different areas in the same sample, showing the dehydrated FeH and 1.5-2.0 nm particles of FeH stabilized by Fe$^{(II)}$ ions. The inset shows a typical SAED pattern, confirming the absence of long-range order.

Upon exposure of the FeH-Fe$^{(II)}$ nanoparticle suspension to NH$_3$ vapor, the pH
5 curve showed an increase with two local maxima (bumps), the first one at pH ~7.5 and the second one at pH ~8.7 (**Figure 4**), suggesting a two-step conversion process involving the uptake of base. Cryo-TEM revealed that the first bump in the pH curve after ~1 hour corresponds to the formation of hexagonal crystals with diameters of 200-500 nm (**Figure 5a**), which on the basis of low-dose SAED (inset) was
10 tentatively identified as green rust, Fe$^{(II)}_3$Fe$^{(III)}$(OH)$_8$Cl.H$_2$O.[19] A more detailed inspection of these hexagonal crystals showed cracks, suggestive of a dissolution process ongoing in parallel to their formation.
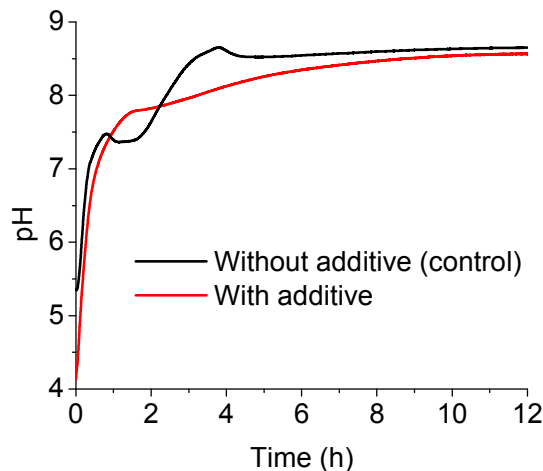


**Figure 4:** pH curves in time for magnetite synthesis from FeH and Fe$^{(II)}$ by NH$_3$ in-diffusion in the
15 absence (control, black) and presence (red) of the additive **EKA**.

Interestingly, both the surfaces and the edges of these disintegrating crystals were covered with particles that from the obtained cryo-TEM images were determined to be 1.0-1.5 nm in size (**Figure 5b**). Although these values are smaller than those quoted for the FeH-Fe$^{(II)}$ particles described above, it is important to stress that the
20 Fresnel fringes associated to the defocus values used to visualize these particles do not allow us to make a definite distinction between the two observed populations. Unfortunately, their co-localization with the green rust crystals also prohibited their further detailed structural analysis with SAED. After the second bump in the pH curve (~4 hours), magnetite crystals started to form on the hexagonal platelets and
25 eventually became the single product, at the expense of both the platelets and nanoparticles present (**Figure 5c,d**).
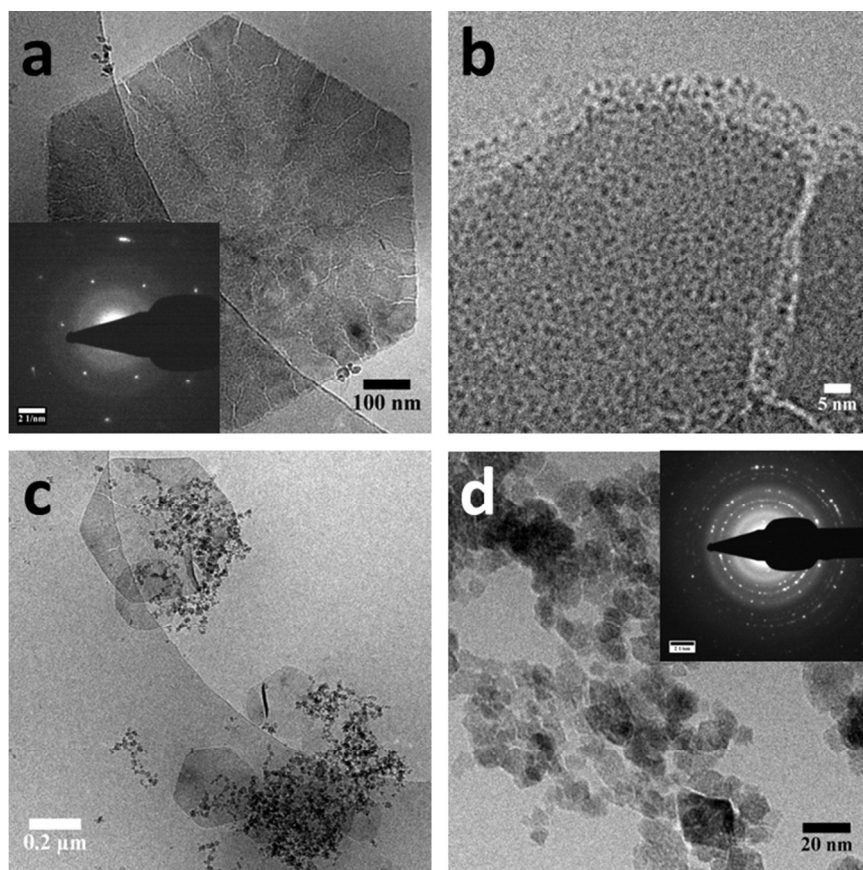
**Figure 5:** Cryo-TEM images of the control experiment. (a) Typical example of a hexagonal crystal of green rust after ~1 hour reaction time. The inset shows the corresponding SAED pattern with 3.9 nm$^{-1}$ spacings.[19] (b) Higher-magnification image of a corner of the green rust crystal in (a), revealing it is covered with spherical nanoparticles, suggesting that the green rust is converting into these particles. (c) Co-localized formation of magnetite (product) near the green rust (intermediate) after ~4 hours reaction time. (d) The final product consists of polydisperse magnetite nanoparticles, rarely showing an octahedral morphology. The inset shows a typical SAED pattern, displaying the common reflections.

More information on these events was obtained when the reaction was performed at a 4-fold higher Fe$^{(II)}$ concentration. Now the cryo-TEM images showed hexagonal platelets with highly corrugated surfaces covered with large numbers of nanometer-sized particles of which the diameters were again measured to be 1.0-1.5 nm (**Figure 6a**). These images suggest that the particles actually are formed by the dissolution of the hexagonal crystals rather than the crystals being formed through the accretion of these particles. Moreover, the cryo-TEM images also showed what seems to be the next step in the crystallization process, i.e. the formation of magnetite through the accretion of the 1.0-1.5 nm particles (**Figure 6b,c,d**), similar to what was reported previously.[14]
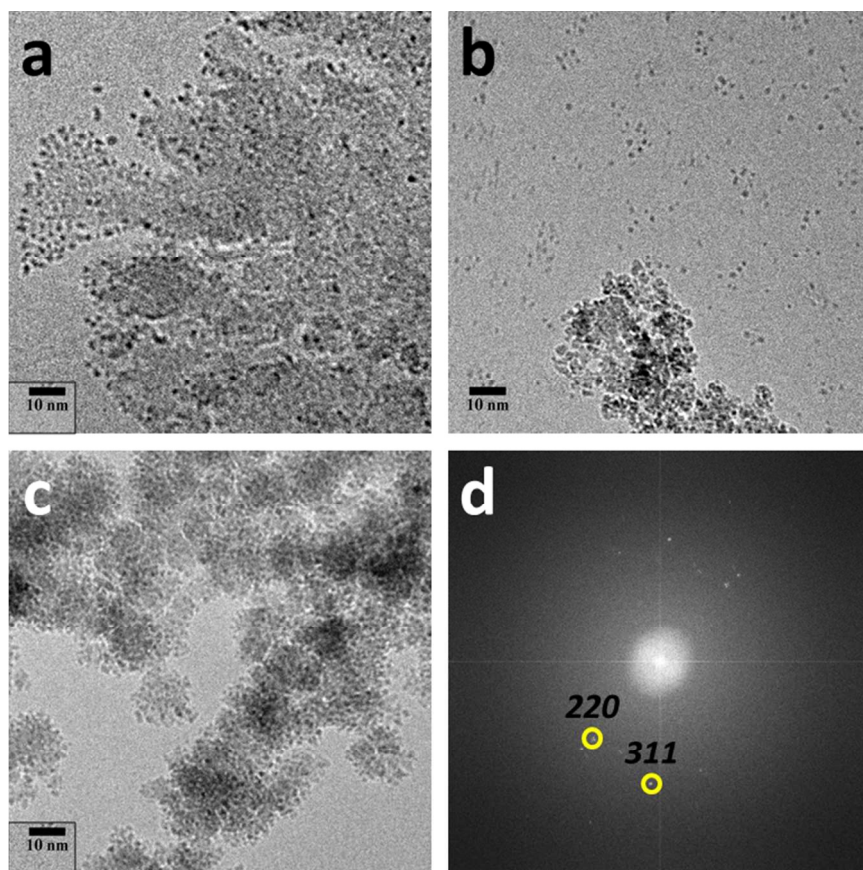
**Figure 6:** Cryo-TEM images of the control experiment at a 4-fold higher $Fe^{(II)}$ concentration. (a) Formation of monodisperse 1.0-1.5 nm particles through green rust dissolution. (b) Formation of magnetite from these nanoparticles. (c) The product consists of magnetite crystals surface-decorated with nanoparticles. (d) FFT of (c), confirming the presence of magnetite crystal planes.

When the mineralization reaction was carried out in the presence of a random copolymer of glutamic acid (E: ~40 mol%), lysine (K: ~30 mol%) and alanine (A: ~30mol%) (**EKA**),[20] the PXRD analysis of the final magnetite crystals showed significant peak broadening (**Figure 1d**), suggesting a decrease in particle size, which was indeed confirmed by cryo-TEM (**Figure 7b**). However, the most remarkable effect of the polypeptide additive was the difference in the phase transformation sequence. The pH curve did no longer display discrete local maxima (**Figure 4**), but showed a transition point after ~1.5 hours at pH ~7.8, followed by a gradual further increase until pH ~8.5. Cryo-TEM showed that the transition point at pH ~7.8 marked the assembly of the 1.5-2.0 nm particles into aggregates for which SAED indicated no long-range order (**Figure 8a**). Although this transition point (a discontinuation in the increase of the pH during the continuous influx of $NH_3$) is indicative of a phase transition, only in a later stage (>12 hours) cryo-TEM with SAED confirmed the presence of crystalline magnetite (**Figure 8b**).
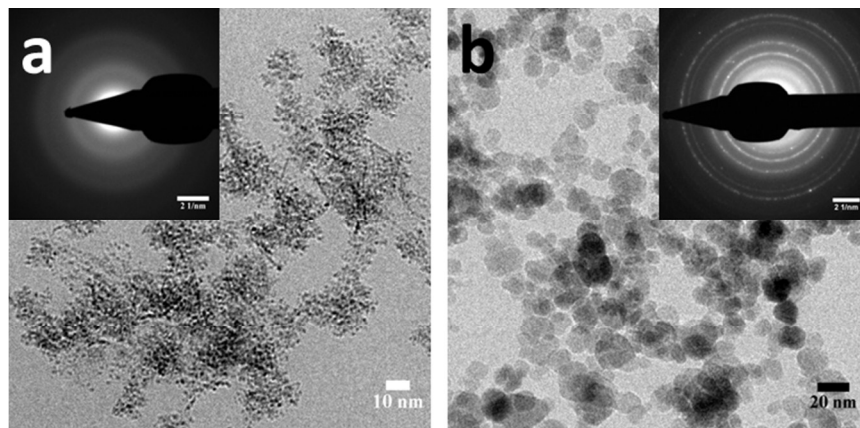
**Figure 7:** Cryo-TEM images of the experiment in the presence of the additive **EKA**. (a) Assembly of the 1.5-2.0 nm particles into aggregates after ~1.5 hours reaction time. The inset shows a typical SAED pattern, confirming the absence of long-range order. (b) The final product after >12 hours reaction time consists of smaller and more uniform magnetite nanoparticles as compared to the control. The inset shows a typical SAED pattern, displaying the 6 major reflections.

## 3 Discussion

Here we show the formation of magnetite by reacting ferrihydrite (FeH) with $Fe^{(II)}$ under the influx of ammonia. Upon exposure of FeH to $Fe^{(II)}$ ions (0.55 equivalent) monodisperse FeH-$Fe^{(II)}$ nanoparticles with dimensions of 1.5-2.0 nm are formed, which we previously have termed primary particles. These primary particles show, in addition to the more monodisperse size distribution, also an increased stability in the electron beam compared to the gel-like FeH phase they nucleate from. The observation of a monodisperse particle size suggests that the interaction of FeH with the ferrous and chloride ions results in FeH-$Fe^{(II)}$ nanoparticles with a specific composition that favors this well-defined size distribution, while the improved stability against electron beam irradiation suggests that this surface reaction is accompanied by dehydration of the original FeH nanoparticles.

Upon increasing the pH we find a next solid intermediate phase, consisting of single-crystalline hexagonal platelets, which we tentatively identified as green rust. Judged from the local minimum observed in the pH curve, the platelets are formed by a discrete nucleation event. The observation of large numbers of nanometer-sized particles attached to their surfaces – and of thinner areas on the crystal surfaces where discrete primary particles can no longer be observed – is suggestive of an accretion-based growth process in which the $Fe^{(III)}$-rich primary particles react with ferrous hydroxide species that become increasingly insoluble when the pH increases above 7.

However, the "fjord"-like cracks in the observed in the plate-like crystals suggests that already during their growth they are disintegrating, a process that was even more prominently observed at higher $Fe^{(II)}$ concentrations (2.2 equivalent with respect to $Fe^{(III)}$). Images showing the disintegrating platelets also reveal their close association with apparently even smaller (1.0-1.5 nm) nanoparticles, which are located both on what used to be the platelet surfaces as well as on the inside of the "fjords". We tentatively interpret these observations as showing the disintegration of the hexagonal plates due to a reaction with the excess primary particles, yielding

smaller secondary particles with a higher $Fe^{(II)}$ content and a lower degree of hydration. Interestingly, we previously observed a similar shrinkage from ~2 nm to ~1 nm in size for primary particles attaching to the surface of magnetite.

The next step in the process is the formation of magnetite, which according to the
5 second bump in the pH curve is again a discrete nucleation event. The cryo-TEM images show that the magnetite nanocrystals form on the surfaces of the hexagonal platelets and grow through the accretion of similar nanometer-sized particles. Although is it difficult to differentiate between the sizes of the primary particles (estimated 1.5-2.0 nm) and the secondary particles (estimated 1.0-1.5 nm) in the
10 current cryo-TEM images, we propose that it is the secondary particles with an increased $Fe^{(II)}/Fe^{(III)}$ ratio still adsorbed on the hexagonal platelets that form the feedstock for magnetite nucleation and growth.

Strikingly, the addition of a polypeptide composed of almost equal amounts of acidic (Glu), basic (Lys) and neutral (Ala) amino acids (**EKA**) let to a quite different
15 crystallization mechanism in which the formation of green rust was completely bypassed. Apart from a transition point at pH ~7.8 in the pH curve, which marked the aggregation of the FeH-$Fe^{(II)}$ primary particles, no further signs of a specific nucleation point was observed, despite the fact that magnetite with a less polydisperse size distribution compared to the control was isolated as the single
20 product. Although acidic polypeptides have been shown to bind both $Fe^{(II)}$ and $Fe^{(III)}$,[16] is unlikely that **EKA** effectively competes with the formation of ferrihydrite above pH ~5. However it is likely that **EKA** binds the far more soluble $Fe^{(II)}$, thereby effectively inhibiting the formation of the green rust at pH 7.5. Nevertheless, as the pH increases to ~7.8, it may no longer be able to prevent the reaction of $Fe^{(II)}$
25 ions with the primary particles. We propose that this results in the formation of the secondary particles, which form aggregates that one by one, possibly depending on the aggregate size, will transform into magnetite through the uptake of ferrous hydroxyl species. Given the fact that magnetite nanocrystals with a more narrow size distribution were formed, the absence of a distinct nucleation event suggests that the
30 nucleation of magnetite must occur from FeH-$Fe^{(II)}$ aggregates that in dimensions are already close to the final crystals, and that the size of the latter is mostly determined by the nucleation event, rather than through a growth process. Although it seems very likely that the same aggregate-to-crystal formation also occurs in the absence of the additive, but the observation of a clear nucleation point for magnetite
35 is observed suggests that the shape and transformation kinetics of the aggregates is modulated through their interaction with the green rust platelets.

## 4 Conclusion

Starting from ferrihydrite (FeH), we have demonstrated the formation of magnetite through a multi-step nucleation process mediated by primary particles that are
40 stabilized by the interaction with $Fe^{(II)}$ ions. We propose that through their interaction with a transient green rust phase the primary particles transform into secondary particles with increased $Fe^{(II)}$ content and reduced hydration levels, which form the feedstock for magnetite formation. Furthermore, it was demonstrated that the presence of an iron-binding polypeptide additive **EKA** prevents the formation of
45 green rust as a $Fe^{(II)}$-rich intermediate phase, and that this leads to the formation of amorphous aggregates of FeH-$Fe^{(II)}$ particles which eventually transform into the final magnetite nanocrystals.

The observation of multiple transitions in the conversion of ferrihydrite to magnetite upon reaction with $Fe^{(II)}$ ions and the involvement of disordered precursor phases is of importance for our understanding of the nucleation of this important magnetic material in geological and biological environments and may lead to new
5 approaches in the sustainable synthesis of this technologically important mineral. Our study further shows the power of cryo-TEM in revealing the development of structure and morphology at the nanoscopic level.

## 5 Acknowledgements

## 6 Experimental

### Synthesis of Ferrihydrite and Magnetite

15 A literature procedure was modified for the syntheses in this manuscript.[17] Ferrihydrite (FeH) was obtained by the addition of 200 mM NaOH solution at a rate of 1 mL/min to 50 mL of 40 mM $FeCl_3.6H_2O$ solution until a pH of 7.5 was reached. This reaction was carried out in glass beaker under stirring and the pH was monitored using a computer-controlled commercial titration setup (Metrohm). A
20 stock solution was prepared from the obtained dispersion by dilution and stored at 4° C for further use.

For magnetite synthesis, 25 mL of the diluted FeH dispersion (2.5 mM $Fe^{(III)}$) was degassed (10-15 min) with $N_2$ flow, followed by the addition of 7.0 mg $FeCl_2.4H_2O$ (1.4 mM $Fe^{(II)}$) and 650 µL $E_{40}K_{30}A_{30}$ (stock solution: 3.33 mg/mL, degassed with
25 $N_2$). For increasing the pH, a 6 vol% $NH_3$ solution was used inside a glove box under $N_2$ atmosphere and constant stirring to keep a homogeneous pH gradient in the reaction mixture. During the in-diffusion of $NH_3$ the pH was monitored using a computer-controlled commercial titration setup (Metrohm).

### Powder X-ray Diffraction (PXRD)

30 PXRD measurements were performed on a Rigaku Geigerflex powder diffractometer with Bragg-Brentano geometry using copper radiation at 40 kV and 30 mA and a graphite monochromator to eliminate Cu $K_\beta$ radiation. Samples were prepared on cover glasses from dried ground powder. The PXRD patterns were acquired by step scans from $2\theta = 20°$ to $2\theta = 70°$ with step sizes of $0.01° – 0.02°$ and an appropriate
35 dwell time.

### (Cryogenic) Transmission Electron Microscopy (Cryo-TEM)

For standard dry TEM, 200 mesh Cu grids with continuous carbon films (Agar Scientific) were used. Sample preparation involved dropping 3 µL aqueous dispersion onto a TEM grid, blotting using filter paper and allowing the grid to dry
40 to the air. For cryo-TEM, 200 mesh Cu grids with Quantifoil R 2/2 holey carbon films (Quantifoil Micro Tools GmbH) were used. Sample preparation was performed using an automated vitrification robot (FEI Vitrobot Mark III) for plunging in liquid ethane.[21] All TEM grids were surface plasma treated for 40 seconds using a

Cressington 208 carbon coater prior to use. TEM samples were studied on a FEI Technai 20 (type Sphera) operated at 200 kV, equipped with a LaB$_6$ filament and a 1k x 1k Gatan CCD camera, or on the TU/e cryoTITAN (FEI, www.cryotem.nl) operated at 300 kV, equipped with a field emission gun (FEG), a post-column Gatan Energy Filter (GIF) and a post-GIF 2k x 2k Gatan CCD camera. Gatan DigitalMicrograph (including DiffTools) and ImageJ were used for TEM image and SAED pattern analysis.

## 7 References

$^a$ *Laboratory of Materials and Interface Chemistry and Soft Matter CryoTEM Research Unit, Department of Chemical Engineering and Chemistry, Eindhoven University of Technology, P.O. Box 513, 5600 MB Eindhoven, The Netherlands. E-mail: N.Sommerdijk@tue.nl*
$^b$ *Institute for Complex Molecular Systems, Eindhoven University of Technology, P.O. Box 513, 5600 MB Eindhoven, The Netherlands.*

1.  R. M. Cornell and U. Schwertmann, *The Iron Oxides (Structure, Properties, Reactions, Occurences and Uses)*, Wiley-VCH, Weinheim, 2003.
2.  C. T. Yavuz, J. T. Mayo, W. W. Yu, A. Prakash, J. C. Falkner, S. Yean, L. Cong, H. J. Shipley, A. Kan, M. Tomson, D. Natelson and V. L. Colvin, *Science*, 2006, **314**, 964-967.
3.  S. Laurent, D. Forge, M. Port, A. Roch, C. Robic, L. Vander Elst and R. N. Muller, *Chem. Rev.*, 2008, **108**, 2064-2110.
4.  A.-H. Lu, E. L. Salabas and F. Schüth, *Angewandte Chemie International Edition*, 2007, **46**, 1222-1244.
5.  D. Faivre and D. Schüler, *Chemical Reviews*, 2008, **108**, 4875-4898.
6.  T. Prozorov, D. A. Bazylinski, S. K. Mallapragada and R. Prozorov, *Materials Science and Engineering: R: Reports*, 2013, **74**, 133-172.
7.  R. Blakemore, *Science*, 1975, **190**, 377-379.
8.  R. B. Frankel, G. C. Papaefthymiou, R. P. Blakemore and W. O'Brien, *Biochimica et Biophysica Acta (BBA) - Molecular Cell Research*, 1983, **763**, 147-159.
9.  D. Faivre, L. H. Böttger, B. F. Matzanke and D. Schüler, *Angewandte Chemie International Edition*, 2007, **46**, 8495-8499.
10. S. Staniland, B. Ward, A. Harrison, G. van der Laan and N. Telling, *Proceedings of the National Academy of Sciences*, 2007, **104**, 19524-19528.
11. J. Baumgartner, G. Morin, N. Menguy, T. Perez Gonzalez, M. Widdrat, J. Cosmidis and D. Faivre, *Proceedings of the National Academy of Sciences*, 2013, **110**, 14883-14888.
12. M. L. Fdez-Gubieda, A. Muela, J. Alonso, A. García-Prieto, L. Olivi, R. Fernández-Pacheco and J. M. Barandiarán, *ACS Nano*, 2013, **7**, 3297-3305.
13. M. I. Siponen, P. Legrand, M. Widdrat, S. R. Jones, W.-J. Zhang, M. C. Y. Chang, D. Faivre, P. Arnoux and D. Pignol, *Nature*, 2013, **502**, 681-684.
14. J. Baumgartner, A. Dey, P. H. H. Bomans, C. Le Coadou, P. Fratzl, N. A. J. M. Sommerdijk and D. Faivre, *Nature Materials*, 2013, **12**, 310-314.
15. J. J. M. Lenders, C. L. Altan, P. H. H. Bomans, A. Arakaki, S. Bucak, G. de With and N. A. J. M. Sommerdijk, *Crystal Growth & Design*, 2014, **14**, 5561-5568.
16. J. J. M. Lenders, H. R. Zope, A. Yamagishi, P. H. H. Bomans, A. Arakaki, A. Kros, G. de With and N. A. J. M. Sommerdijk, *Advanced Functional Materials*, 2014, accepted.
17. H. Liu, M. Ma, M. Qin, L. Yang and Y. Wei, *J. Solid State Chem.*, 2010, **183**, 2045-2050.
18. H. Friedrich, P. M. Frederik, G. de With and N. A. J. M. Sommerdijk, *Angewandte Chemie International Edition*, 2010, **49**, 7850-7858.

19.  I. R. McGill, B. McEnaney and D. C. Smith, *Nature*, 1976, **259**, 200-201.
20.  V. Dmitrović, J. J. M. Lenders, H. R. Zope, G. de With, A. Kros and N. A. J. M. Sommerdijk, *Biomacromolecules*, 2014, **15**, 3687-3695.
21.  M. R. Vos, P. H. H. Bomans, P. M. Frederik and N. A. J. M. Sommerdijk, *Ultramicroscopy*, 2008, **108**, 1478-1483.